

## Thickness dependent red shift of the photocurrent spectrum in bulk heterojunction solar cells

B. K. Abeyweera and B. W. Alphenaar

Citation: [Applied Physics Letters](#) **102**, 041113 (2013); doi: 10.1063/1.4789905

View online: <http://dx.doi.org/10.1063/1.4789905>

View Table of Contents: <http://scitation.aip.org/content/aip/journal/apl/102/4?ver=pdfcov>

Published by the [AIP Publishing](#)

---

### Articles you may be interested in

[Investigating the origin of S-shaped photocurrent-voltage characteristics of polymer:fullerene bulk-heterojunction organic solar cells](#)

[J. Appl. Phys.](#) **115**, 124504 (2014); 10.1063/1.4869661

[Fluctuations in photocurrent of bulk heterojunction polymer solar cells—A valuable tool to understand microscopic and degradation processes](#)

[Appl. Phys. Lett.](#) **101**, 043903 (2012); 10.1063/1.4738985

[Enhanced charge collection in confined bulk heterojunction organic solar cells](#)

[Appl. Phys. Lett.](#) **99**, 163301 (2011); 10.1063/1.3651509

[Modeling of bulk and bilayer organic heterojunction solar cells](#)

[Appl. Phys. Lett.](#) **96**, 143307 (2010); 10.1063/1.3383232

[Enhancing the photocurrent in poly\(3-hexylthiophene\)/\[6,6\]-phenyl C 61 butyric acid methyl ester bulk heterojunction solar cells by using poly\(3-hexylthiophene\) as a buffer layer](#)

[Appl. Phys. Lett.](#) **95**, 133303 (2009); 10.1063/1.3242006

---

The advertisement features a row of tablet computers displaying the journal's cover. The cover art shows a colorful, swirling pattern. The journal title 'Computing' is at the top, and 'AIP'S JOURNAL OF COMPUTATIONAL TOOLS AND METHODS' is at the bottom. The text 'AVAILABLE AT MOST LIBRARIES.' is prominently displayed in large white letters at the bottom of the image. The 'computing' logo with 'IN SCIENCE & ENGINEERING' is in the bottom right corner.

**computing**  
IN SCIENCE & ENGINEERING

AIP'S JOURNAL OF COMPUTATIONAL TOOLS AND METHODS.  
**AVAILABLE AT MOST LIBRARIES.**

## Thickness dependent red shift of the photocurrent spectrum in bulk heterojunction solar cells

B. K. Abeyweera and B. W. Alphenaar

Department of Electrical and Computer Engineering, University of Louisville, Louisville, Kentucky 40292, USA

(Received 5 October 2012; accepted 16 January 2013; published online 30 January 2013)

Photocurrent spectra are measured for two different types of bulk heterojunction organic solar cells having a range of active layer thicknesses. Normalized by the number of incident photons, the photocurrent peak red shifts with respect to the absorption maximum as the sample thickness increases. Comparison to photocurrent measurements made with a chopped light source shows that the shift is due to an increased contribution from long wavelength absorption in the central active region. Fitting the thickness dependent photocurrent to a charge recombination model provides a measure of carrier collection lengths and surface recombination. © 2013 American Institute of Physics. [<http://dx.doi.org/10.1063/1.4789905>]

The optimum thickness for the active layer of an organic solar cell is determined by a balance between two or more competing effects. To maximize absorption, the product of the active layer thickness  $d$  and the wavelength dependent absorption coefficient  $\alpha(\lambda)$  should be greater than unity. However, if  $d$  is too large, the efficiency is reduced because of the low carrier collection lengths in organic materials and bi-molecular recombination processes.<sup>1,2</sup> To maximize efficiency,  $d$  is generally kept below 100 nm.<sup>3</sup> The disadvantage of such thin layers is that the photocurrent is absorption limited for a range of wavelengths and much of the incident light outside peak values for  $\alpha(\lambda)$  is lost.

In this Letter, the dc photocurrent spectrum is compared for organic solar cells having active layers of increasing thicknesses. As the sample thickness is increased, an increasing percentage of light away from the absorption maximum contributes to the photocurrent due to carriers generated in the bulk of the sample. While fewer in number, these carriers can have an undue influence on the photocurrent. This is because they do not suffer from some of the same loss mechanisms that affect carriers generated on the surface. For example, bimolecular recombination mainly influences charge generated near the top contact, where the charge concentration is highest. Also, excitons generated within an exciton diffusion length ( $<20$  nm)<sup>4</sup> of the surface can recombine through contact interface states prior to dissociation. Finally, electrons generated at the front hole-collecting contact interface must diffuse the entire length of the sample before reaching the back contact and can recombine before being collected. By measuring samples whose active layer thickness is above the optimum value, it is possible to obtain a comparison of photocurrent collected from carriers generated in the bulk of the sample versus those generated at the surface. This then provides a measure of the electron collection length and the surface enhanced recombination.

Two different conjugated polymers were used in these experiments: poly(2-methoxy-5-[3,7-dimethyloctyloxy]-1,4-phenylenevinylene (MDMO-PPV) and regioregular poly(3-hexylthiophene) (P3HT). These were purchased from Sigma Aldrich Co. and Nano-C Inc., respectively. Solar cell device structures were made according to the standard procedure described in the literature.<sup>5,6</sup> First, a 30 nm thick

PEDOT-PSS poly(3,4-ethylenedioxythiophene) poly(styrenesulfonate) contact layer was spin coated onto a clean indium tin oxide (ITO) coated glass substrate, and the sample baked at 140 °C for 10 min. Next, the active layer spin coated onto the contact layer in a N<sub>2</sub> filled glove box. Active layer weight ratios were 1:4 MDMO-PPV/PCBM [6,6]-phenyl-C61-butyric acid methyl ester in 1,2-Dichlorobenzene anhydrous and 5:4 P3HT/PCBM in 99.9% Chlorobenzene. After annealing at 100 °C for 30 min in N<sub>2</sub>, the sample was inserted into an e-beam evaporator, and the top contact deposited (1 nm LiF/60 nm Al). The samples were then loaded into a N<sub>2</sub> filled optical cryostat for measurements.

Figures 1(a) and 1(b) show the absorption coefficients of the P3HT:PCBM and MDMO-PPV:PCBM active layers, respectively. Measurements were made using a Varian Cary

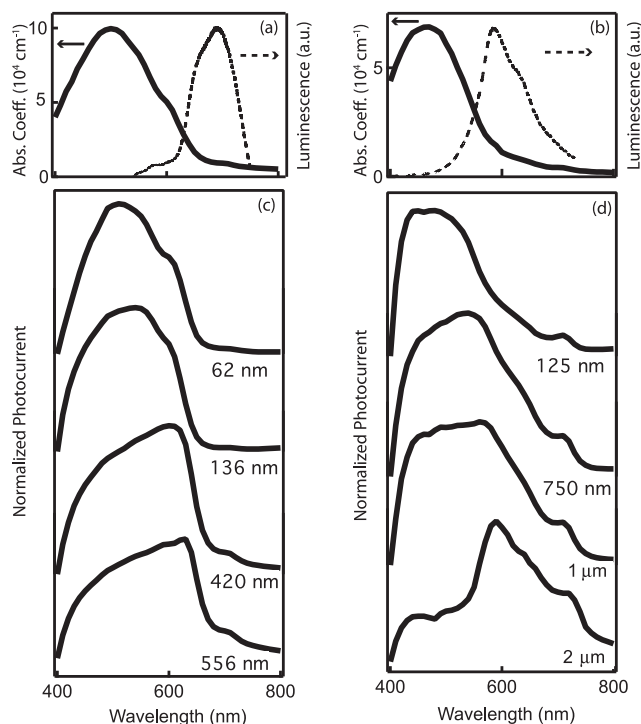


FIG. 1. (a) Absorbance and luminescence spectrum for P3HT and for (b) MDMO-PPV. (c) Photocurrent spectra for 4 different active layer thickness of P3HT/PCBM and (d) MDMO-PPV/PCBM solar cells.

50 UV-VIS Spectrophotometer using films spin coated onto a glass slide. Measurements were made for samples of varying thicknesses, and each produced a similar wavelength dependence, with no apparent interference effects. P3HT:PCBM has an absorption maximum of  $10 \times 10^4 \text{ cm}^{-1}$  at 500 nm, while MDMO-PPV has a somewhat lower absorption maximum  $6.9 \times 10^4 \text{ cm}^{-1}$  at 470 nm.<sup>7,8</sup> Also shown are the photoluminescence spectra of P3HT (Fig. 1(a)) and MDMO-PPV (Fig. 1(b)), measured under 325 nm excitation from a He-Cd laser using a Renishaw RL633 spectrometer. As is typically observed, there is a Stokes shift between the absorbance and luminescence spectra due to the thermalization of absorbed carriers to the lower energy states near the band edge prior to radiative recombination.<sup>9</sup>

Figure 1(c) shows the photocurrent spectra for 4 different P3HT:PCBM solar cells having different active layer thicknesses. The dc photocurrent was measured in the short circuit condition with continuous light incident on the ITO contact. The light source is a QTH 1000 W lamp resolved in the visible region by a SpectraPro (500i) monochromator (Acton Research). The active region thicknesses were determined using a Dektak profilometer. The signal is normalized by dividing the photocurrent by the number of incident photons (determined by measuring the power output from the light source). Because the total current tends to decrease as the sample thickness increases (with sample-to-sample fluctuations), each trace is also normalized to its peak photocurrent so that the wavelength dependence for different active layer thicknesses can be easily compared.

For the thinnest samples, the photocurrent spectrum roughly matches with the absorption spectrum, with the peak photocurrent occurring at the same wavelength as the peak in  $\alpha(\lambda)$ . As the active layer thickness increases, the maximum in the photocurrent peak shifts to longer wavelengths. Eventually, for the thickest samples, the photocurrent peak is more closely aligned with the luminescence peak than with the absorption peak. Figure 1(d) shows a similar set of spectra for MDMO-PPV:PCBM solar cells of increasing active layer thickness. Once again, the photocurrent peak matches the peak in the absorption spectrum in the thinnest sample, but red shifts to match the peak in the luminescence spectrum for the thickest sample. A larger sample thickness variation is required to observe the shift in MDMO-PPV samples than in P3HT samples. This is due to the lower absorption coefficient of MDMO-PPV. Note that a small feature is observed at 700 nm that remains fixed in all of the samples. This peak is due to the PCBM S1 transition and provides a fixed reference for comparison.

These results are surprising because it is generally reported that the photocurrent maximum occurs at the maximum of the absorption coefficient, irrespective of the sample thickness. One difference is that here the photocurrent is measured using a continuous light source, rather than using a chopped light source as is often done. A comparison between the photocurrent measured with continuous and chopped light sources for the thickest samples is shown in Fig. 2(a) for the P3HT:PCBM device and Fig. 2(b) for the MDMO-PPV:PCBM device. The light source is chopped at 2 kHz, and the resulting ac short circuit current is measured using a lock-in amplifier.<sup>10</sup> Once again the signal is normalized by

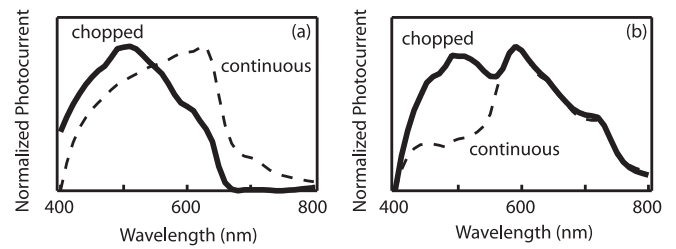


FIG. 2. Photocurrent spectra for the thickest samples shown in Fig. 1, measured using a light source chopped at 2 kHz for (a) P3HT/PCBM and (b) MDMO-PPV/PCBM solar cells. For comparison, the photocurrent spectra measured using a continuous light source are also shown (dashed lines).

the incident number of photons and plotted with respect to the peak photocurrent value. As seen in Fig. 2, the ac photocurrent has a peak corresponding to the absorbance maximum, even when the active layer is thick. The difference between the continuous and chopped spectra is particularly pronounced for the P3HT samples. In both cases, a feature corresponding to the continuous photocurrent peak is still apparent in the chopped spectrum. This suggests that the shift in the continuous photocurrent peak with sample thickness is due to a relative enhancement of the contribution from carriers created by long wavelength absorption. These carriers are generated in the bulk of the sample and require a longer time to be collected by the contacts. Hence, in the ac measurement, their contribution diminishes, even at a relatively low frequency of 2 kHz.

The shift in photocurrent peak can be understood by modeling the carrier extraction as a function of sample thickness. Consider the schematic device drawing in the inset to Fig. 3(c). Here, incident light generates a population of electron-hole pairs  $Q(x)dx$  a distance  $x$  from the top (hole collecting) contact. In the standard formulation first described by Hecht,<sup>11,12</sup> the charge extracted from this population decreases exponentially with distance  $x$  due to recombination. The total extracted charge is then determined assuming a constant photogenerated charge density in the active region,  $Q(x) = Q_0/d$ . This approximation can be justified for  $d \ll 1/\alpha$ , however, for thicker samples, we must consider the variation in  $Q(x)$  due to the change in photon absorption with distance,  $Q(x) = Q_0\alpha e^{-\alpha x}$ . Calculating the charge extracted from this population gives<sup>13</sup>

$$\frac{Q_e}{Q_0} = \frac{\alpha e^{-\left(\frac{d}{d_e}\right)}}{\left(\frac{1}{d_e} - \alpha\right)} \left[ e^{d\left(\frac{1}{d_e} - \alpha\right)} - e^{d_s\left(\frac{1}{d_e} - \alpha\right)} \right], \quad (1a)$$

$$\frac{Q_h}{Q_0} = \frac{\alpha}{\left(\frac{1}{d_h} + \alpha\right)} \left[ e^{-d_s\left(\frac{1}{d_h} + \alpha\right)} - e^{-d\left(\frac{1}{d_h} + \alpha\right)} \right], \quad (1b)$$

where  $Q_e$  and  $Q_h$  are the collected electrons and holes, and  $d_e$  and  $d_h$  are the characteristic electron and hole collection lengths. A surface recombination length  $d_s$  is also introduced, where it is assumed that charge generated within a distance  $d_s$  from the top contact is lost due to recombination through contact interface states or bimolecular recombination.

Figure 3 shows  $Q_e/Q_0$  and  $Q_h/Q_0$  as a function of absorption coefficient for (a)  $d = 100$  nm and (b)  $d = 300$  nm. In both cases, we use  $d_e = d_h = 500$  nm and  $d_s = 20$  nm. The calculation shows that the collected charge reaches a maximum value

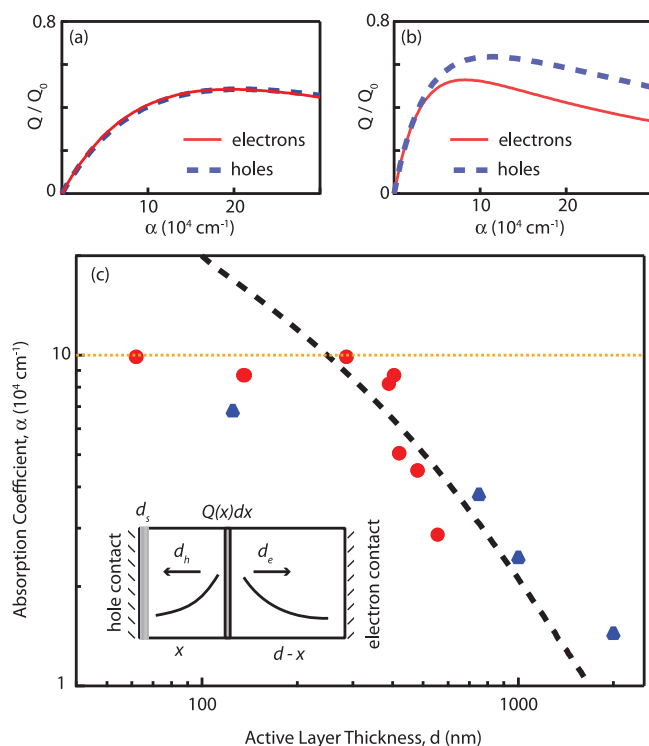


FIG. 3. The fraction of extracted charge as a function of the absorption coefficient for active layer thicknesses of (a) 100 nm and (b) 300 nm. (c) The absorption coefficient measured at the photocurrent peak for various thickness P3HT/PCBM (red circles) and MDMO-PPV/PCBM samples (blue triangles). The dashed line is a fit to the theoretical model for  $d_e = d_h = 500$  nm and  $d_s = 20$  nm, while the dotted line shows the maximum absorption coefficient for P3HT. Inset: Device layout used in the calculation.

at some optimum absorption coefficient ( $19.6 \times 10^4 \text{ cm}^{-1}$  for the 100 nm thick sample and  $8.3 \times 10^4 \text{ cm}^{-1}$  for the 300 nm thick sample) and that this value decreases with increasing sample thickness. For the 100 nm thick sample, the optimum absorption coefficient is higher than the peak absorption coefficient for P3HT or MDMO-PPV. In this situation, the photocurrent peak occurs at the absorption coefficient peak as observed for the thin samples in Fig. 1. For the 300 nm thick sample, the optimum absorption coefficient is lower than the peak absorption coefficient, so that the photocurrent peak is red shifted.

In Fig 3(c), the optimum absorption coefficient corresponding to the maximum value of  $Q_e/Q_0$  is plotted as a function of sample thickness. Also plotted is the absorption coefficient corresponding to the wavelength of the photocurrent peak for P3HT and MDMO-PPV, taken from measurements of solar cells with different active layer thicknesses as shown in Fig. 1. The model provides a good fit for the data

using  $d_e = d_h = 500$  nm and  $d_s = 20$  nm. For thinner P3HT devices, the position of the photocurrent peak stays approximately constant, at the absorption maximum (dotted line) because the optimum absorption coefficient is greater than the absorption maximum. Both P3HT and MDMO-PPV samples are described by the same behavior. This is most likely because in both types of devices the current, which is limited by electron transport, occurs through the PCBM. The carrier recombination length is not well characterized in organic solar cells and estimates range from 500 nm to  $2 \mu\text{m}$ .<sup>14</sup> The analysis here suggests that the correct value is closer to 500 nm; using larger or smaller values for the collection lengths provides a poorer fit to the data.

To conclude, the photocurrent spectra are compared for organic solar cells having active layers of increasing thicknesses. For thin samples, the maximum photocurrent corresponds to the wavelength of the absorption maximum. As the sample thickness increases, the photocurrent maximum shifts to longer wavelength, suggesting that the photocurrent is no longer limited by the absorbance, but is instead limited by recombination processes occurring at the contact interface and electron diffusion. By fitting the absorption coefficient at the photocurrent peak, a measure of the carrier collection length and the percentage of carriers lost to surface recombination are obtained.

This work is funded through the National Science Foundation Grant No. NSF-DMR-0906961 with facilities support from the Conn Center for Renewable Energy Research.

- <sup>1</sup>J. D. Kotlarski, P. W. M. Blom, L. J. A. Koster, M. Lenens, and L. H. Sloff, *J. Appl. Phys.* **103**, 084502 (2008).
- <sup>2</sup>L. J. A. Koster, V. D. Mihailetschi, and P. W. M. Blom, *Appl. Phys. Lett.* **88**, 052104 (2006).
- <sup>3</sup>P. W. M. Blom, V. D. Mihailetschi, L. J. A. Koster, and D. E. Markov, *Adv. Mater.* **19**, 1551 (2007).
- <sup>4</sup>H. Hoppe and N. S. Sariciftci, *J. Mater. Res.* **19**, 1924 (2004).
- <sup>5</sup>W. Y. Ma, C. Gong, X. Lee, and A. J. Heeger, *Adv. Funct. Mater.* **15**, 1617 (2005).
- <sup>6</sup>M. M. Wienk, J. M. Kroon, W. J. Verhees, J. Knol, J. C. Hummelen, P. A. van Hal, and R. A. Janssen, *Angew. Chem., Int. Ed.* **42**, 3371 (2003).
- <sup>7</sup>H. Hoppe, S. Shokhovets, and G. Gobsch, *Phys. Status Solidi (RRL)* **1**, R40 (2007).
- <sup>8</sup>M. Hallermann, I. Kriegel, E. Da Como, J. M. Berger, E. von Hauff, and J. Feldmann, *Adv. Funct. Mater.* **19**, 3662 (2009).
- <sup>9</sup>K. F. Colladet, S. Cleij, T. J. Lutsen, L. Gelan, and J. Vanderzande, *Macromolecules* **40**, 65 (2007).
- <sup>10</sup>J. Y. Kim, K. Lee, N. E. Coates, D. Moses, T. Q. Nguyen, M. Dante, and A. J. Heeger, *Science* **317**, 222 (2007).
- <sup>11</sup>K. Hecht, *Z. Phys. A-Hadrons Nucl.* **77**, 235 (1932).
- <sup>12</sup>R. A. Street and M. Schoendorf, *Phys. Rev. B* **81**, 205307 (2010).
- <sup>13</sup>See supplementary material at <http://dx.doi.org/10.1063/1.4789905> for a more detailed description of the theoretical calculation.
- <sup>14</sup>C. Diebel, *Phys. Status Solidi A* **206**, 2731 (2009).